A cell-based boundary model of gastrulation by unipolar ingression in the hydrozoan cnidarian Clytia hemisphaerica

Maarten van Der Sande, Yulia Kraus, Evelyn Houliston, Jaap Kaandorp

Developmental Biology 460 (2020) 176–186

Contents lists available at ScienceDirect

Developmental Biology

journal homepage: www.elsevier.com/locate/developmentalbiology

A cell-based boundary model of gastrulation by unipolar ingression in the hydrozoan cnidarian *Clytia hemisphaerica*

Maarten van der Sande [a], Yulia Kraus [b,c], Evelyn Houliston [d], Jaap Kaandorp [a,*]

[a] Computational Science Lab, University of Amsterdam, Science Park 904, 1098XH, Amsterdam, the Netherlands
[b] Department of Evolutionary Biology, Lomonosov Moscow State University, Russia
[c] Koltzov Institute of Developmental Biology of the Russian Academy of Sciences, 26 Vavilov Street, Moscow, 119334, Russia
[d] Sorbonne Université, CNRS, Laboratoire de Biologie du Développement de Villefranche-sur-mer (LBDV), 06230, Villefranche-sur-mer, France

ARTICLE INFO

Keywords:
Clytia hemisphaerica
Gastrulation
Ingression
Planar cell polarity
Strabismus
Cell-based model

ABSTRACT

In Cnidaria, modes of gastrulation to produce the two body layers vary greatly between species. In the hydrozoan species *Clytia hemisphaerica* gastrulation involves unipolar ingression of presumptive endoderm cells from an oral domain of the blastula, followed by migration of these cells to fill the blastocoel with concomitant narrowing of the gastrula and elongation along the oral-aboral axis. We developed a 2D computational boundary model capable of simulating the morphogenetic changes during embryonic development from early blastula stage to the end of gastrulation. Cells are modeled as polygons with elastic membranes and cytoplasm, colliding and adhering to other cells, and capable of forming filopodia. With this model we could simulate compaction of the embryo preceding gastrulation, bottle cell formation, ingression, and intercalation between cells of the ingressing presumptive endoderm. We show that embryo elongation is dependent on the number of endodermal cells, low endodermal cell-cell adhesion, and planar cell polarity (PCP). When the strength of PCP is reduced in our model, resultant embryo morphologies closely resemble those reported previously following morpholino-mediated knockdown of the core PCP proteins Strabismus and Frizzled. Based on our results, we postulate that cellular processes of apical constriction, compaction, ingression, and then reduced cell-cell adhesion and mediolateral intercalation in the presumptive endoderm, are required and when combined, sufficient for *Clytia* gastrulation.

1. Introduction

The process of gastrulation sets up the germ layers and fixes the embryonic axes to define the animal body plan. Species of the major animal clade "Bilateria" are triploblastic, and gastrulation creates three germ layers: ectoderm, endoderm and mesoderm. Species in the sister clade Cnidaria are considered "diploblastic", i.e. they have only two germ layers, ectoderm and endoderm (sometimes termed entoderm). Within both Bilateria and Cnidaria the details of gastrulation vary between species, with specific cell populations of the single-layered blastula undergoing, in different combinations, cell sheet invagination, involution and epiboly as well as individual cell delamination and ingression (Gilbert, 2010).

Cnidarian gastrulation includes a rich variety of modes (Kraus and Markov, 2017), of which two extreme modes are seen in the main laboratory model species *Nematostella vectensis* from Anthozoa and *Clytia hemisphaerica* from Hydrozoa. *Nematostella* gastrulation is largely based on invagination of the future "oral" side of the blastoderm corresponding to the presumptive endoderm territory (Kraus and Technau, 2006; Magie and Daly, 2007), while in *Clytia* (= *Phialidium*) species, the endoderm forms entirely from cells detaching individually from the blastoderm at the future oral pole and migrating inward to fill the blastocoel, a process known as unipolar ingression (Byrum, 2001). While *Nematostella* invagination-based gastrulation has been described in detail and simulated (Tamulonis et al., 2011), little is yet known about the mechanical basis of hydrozoan gastrulation by unipolar ingression.

The larva of the hydrozoan model species *Clytia hemisphaerica* is a simple two-layered "planula" with a polarized torpedo shape (Houliston et al., 2010). It swims unidirectionally with its broader "aboral" pole at the front, thanks to coordinated beating of single cilia on each ectodermal cell. The common orientation of the ectoderm cells and thus of the cilia is governed by planar cell polarity (PCP) along the aboral-oral axis, which involves the segregation of the highly conserved transmembrane protein Strabismus to the aboral side of each cell, likely

* Corresponding author.
E-mail address: J.A.Kaandorp@uva.nl (J. Kaandorp).

https://doi.org/10.1016/j.ydbio.2019.12.012
Received 9 July 2019; Received in revised form 9 December 2019; Accepted 21 December 2019
Available online 2 January 2020

interacting with Frizzled 1 protein on the oral side of the adjacent cell (Momose et al., 2012). Polarity is established in the egg, and the germ layers are formed during gastrulation. Gastrulation is completed roughly 24 h after fertilization (hpf), see Fig. 1, the exact timing depending on temperature. Subsequent cell differentiation in both germ layers creates a metamorphosis-competent planula larva on the third day after fertilization. We have recently characterized in detail the cell morphological changes that precede and accompany gastrulation in *Clytia* (Kraus et al. (2019). The period until the end of gastrulation comprises five successive and partially overlapping processes: cleavage, epithelialization, compaction, cell ingression and elongation. During cleavage, repeated divisions transform the fertilized egg into a monolayered blastula. During epithelialization, the cells of the blastula flatten against each other and become polarized along an apicobasal axis to form an epithelium, with cell-cell junctions developing apically. The compaction process, which occurs in parallel with epithelialization, reduces the overall diameter of the embryo while the blastoderm layer increases in thickness. Gastrulation starts at about 11–12 hpf. It involves individual ingression of presumptive endoderm cells into the blastocoel from a domain covering about one third of the blastoderm, centered on the oral pole of the blastula. The ingressing cells fill the blastocoel cavity (Fig. 2). As they migrate towards the aboral pole, the embryo elongates along the oral-aboral axis. Mid-gastrula stage embryos are roughly pear-shaped, with the oral end being narrower and the aboral end more spherical (Fig. 1 16.5h).

At the molecular level we know that the presumptive endoderm territory is established by Wnt/Beta-Catenin signalling prior to gastrulation. The location of this territory is determined by the initial polarzed distribution of Wnt and Fz mRNAs in the egg, which define an oral domain centered around the site of the original egg animal pole, and its extent by feedback interactions along the developing body axis (Momose and Houliston, 2007; Momose et al., 2008). Cells in this domain are fated to become either oral ectoderm or endoderm (Lapébie et al., 2014). The rest of the cells give rise to lateral and aboral ectoderm (Byrum, 2001).

The mechanism of embryo elongation during gastrulation in *Clytia* is not fully understood, but it is likely to involve intercalation between cells perpendicular to the oral-aboral axis, in a similar manner to elongation of chordate embryos by intercalation of involuting mesoderm cells (convergent extension) (Wallingford et al., 2002). Supporting this idea, patches of marked cells in lateral regions become elongated along the

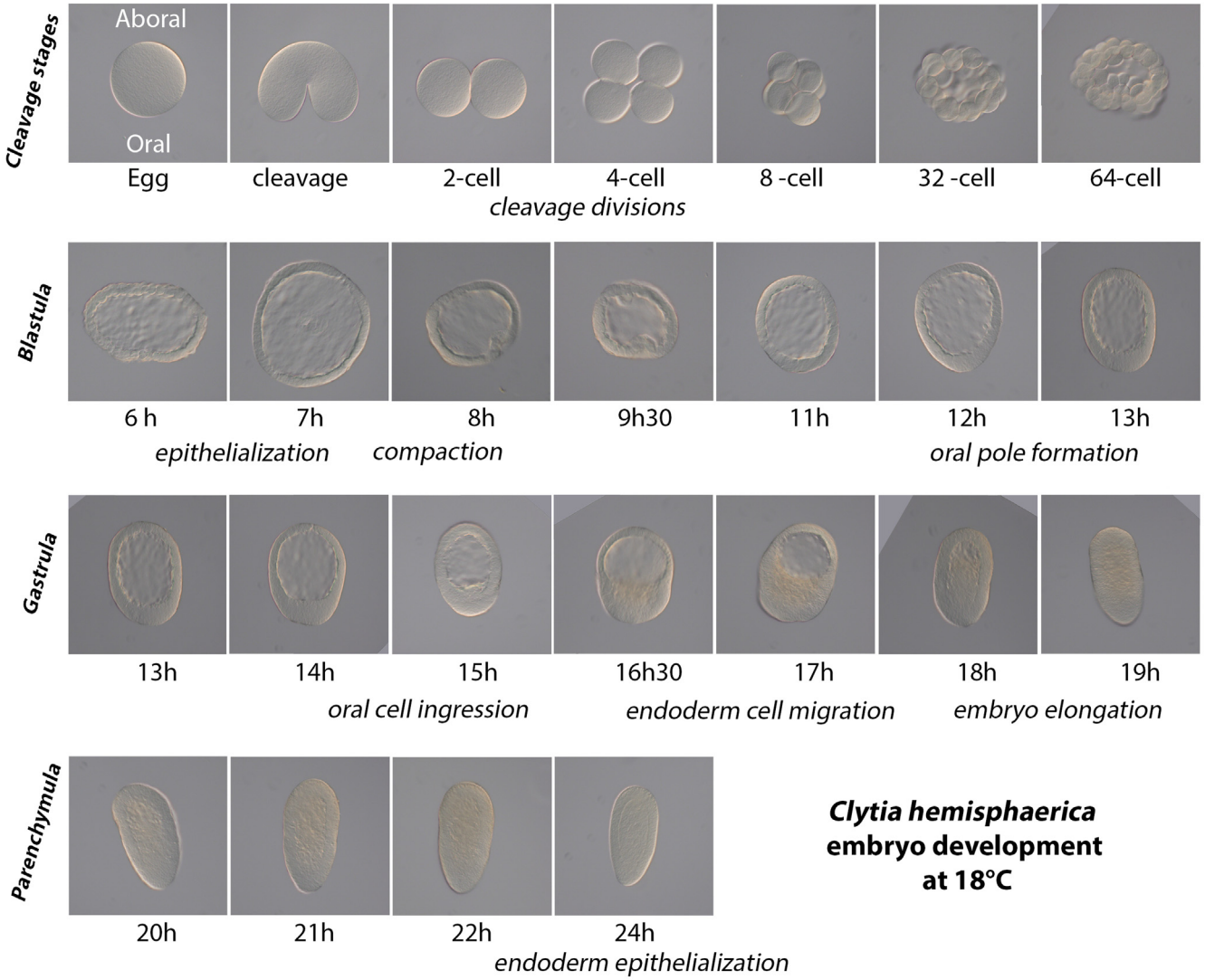

Fig. 1. *Clytia* embryogenesis from egg to the end of gastrulation. DIC images of embryos at successive times post fertilization from a population developing synchronously at 18 °C are shown. Note that the overall morphology of blastula and gastrula stage embryos is quite irregular and can vary considerably between embryos. After the initial cleavage divisions, cells organize into an epithelial sheet and the embryo becomes more compact as each cell polarizes and elongates along its apicobasal axis. Gastrulation starts at around 12 hpf by detachment of cells from the oral domain into the blastocoel. As ingressing cells progressively fill the blastocoel, the developing planula adopts an elongated oval shape.

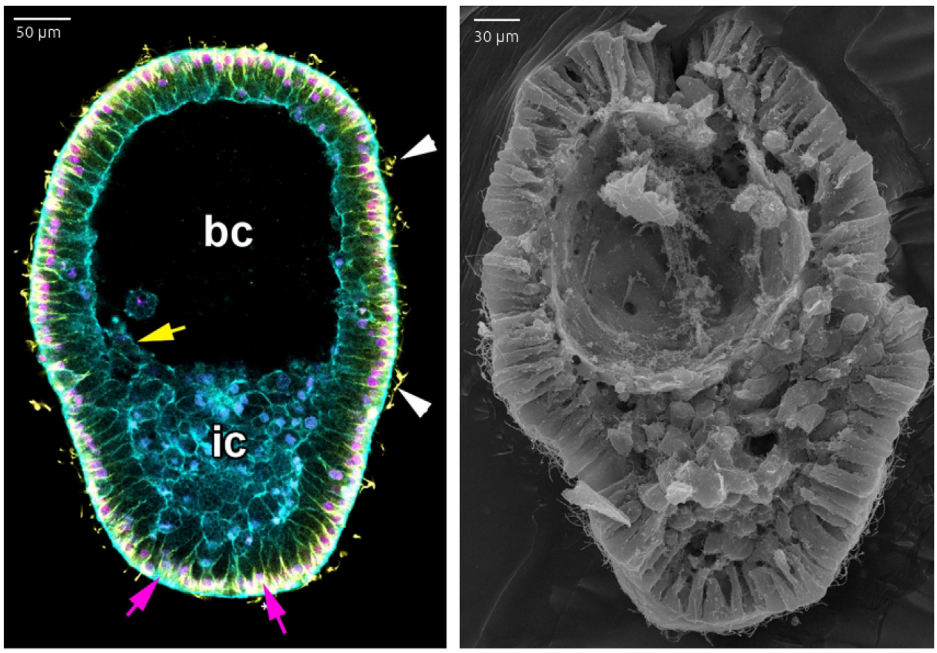

Fig. 2. A: Confocal microscopy of a gastrulating embryo, wih cell boundaries labelled in cyan, nuclei in magenta and microtubules in yellow. The magenta arrows indicate ingressing cells, the yellow arrow indicates an ingressed cell migrating on the blastocoel wall, and white arrows cilia. B: Scanning electron microscopy image of a gastrulating embryo. The oral pole is at the bottom in both panels.

oral-aboral axis and correspondingly narrower during gastrulation (Byrum, 2001). Furthermore, *Clytia hemisphaerica* embryo elongation, like chordate convergent extension, is inhibited by interfering with Planar Cell Polarity, a process mediated by evolutionary conserved PCP proteins (Momose et al., 2012). PCP operates in epithelial tissues in many animals, and is responsible for aligning hairs and cuticle structures made by ectodermal cells, as well as for coordinated cell movements in both epithelial and mesenchymal tissues. Core PCP components are highly conserved, including the transmembrane receptors Frizzled, Flamingo, and Strabismus, and the cytoplasmic proteins Diego, Dishevelled, and Prickle (Lapébie et al., 2011). Knockdown of Strabismus or Dishevelled in *Clytia* by injecting antisense morpholino oligonucleotides prior to fertilization prevents the coordination of cilia orientation in the gastrula and planula ectoderm, and also abrogates embryo elongation during gastrulation, with the zone of oral ingression failing to narrow as gastrulation proceeds.

PCP-dependent cell intercalation relative to the oral-aboral axis in *Clytia* could potentially act in the developing ectoderm, endoderm, or both, to drive embryo elongation during gastrulation. Intercalation of the ectodermal cells would involve changing of their relative positions in the epithelial sheet via lateral interactions, a process well described in other animals involving different epithelial intercalation modes, for instance involving junction remodeling (Walck-Shannon and Hardin, 2014). In contrast, intercalation of the ingressing mesenchymal endoderm cells would be analogous to presumptive mesoderm cells during chordate embryo convergent extension, which form strong mediolateral bonds with their neighboring cells and generate traction on these bonds. This traction is responsible for the tissue narrowing, and consequently elongation perpendicular to the direction of the bonds (Wallingford et al., 2002). In another hydrozoan species, *Podocoryne carnea*, the embryo elongates before ingression begins (Momose and Schmid, 2006), indicating that intercalation between the presumptive ectodermal epithelial cells can drive elongation.

We designed a cell-based model to understand better the cellular dynamics and forces at play during gastrulation of *Clytia*. Many different types of cell-based models exist for morphogenetic processes such as this, each with their own advantages and constraints. Typically, cellular-Potts or vertex models are used to model cell-cell interactions. The cellular-Potts model first was used to model cell-sorting (Graner and Glazier, 1992), but has since been used to model tissue growth (Szabó and Merks, 2013), migration (Marco Scianna and Preziosi, 2013), and development (Marco Scianna and Preziosi, 2013). Its simple design makes it an attractive, and easy to understand model, however also limits the forces and interactions it can model. In vertex models, the cell is represented by a set of vertices that mark the intersection of two or more neighboring cells. One of the earliest vertex models simulated different types of cell sheet invagination, like neural tube formation, ventral furrow formation, and exogastrulation (Odell et al., 1981). A disadvantage of these kinds of models is their constraint that cells must form a continuous sheet, from which they cannot detach.

Previously we devised a cell-based boundary model of *Nematostella* embryogenesis which successfully describes its gastrulation, including cell sheet invagination, zippering, and the forming of bottle cells (Tamulonis et al., 2011). We report that with small changes to the original model developed for *Nematostella* we can describe the successive processes observed during the development of *Clytia* embryos. This model also allowed us to test the influence of several factors, such as planar cell polarity, on the morphological changes of gastrulation.

2. Materials and Methods

Embryos from *Clytia hemisphaerica* laboratory Z strains (Leclère et al., 2019) were used for all experiments. DIC images of live embryos were taken on an Olympus BX51 microscope. Fluorescence staining and confocal imaging of fixed embryos stained with Hoechst dye (for DNA), Rhodamine-phalloidin (for cell boundaries) and anti-tubulin (rat monoclonal YL1/2), was performed exactly as described previously, using a Leica SP5 microscope (Lapébie et al., 2014).

For scanning electron microscopy (SEM) embryos were fixed in the following fixative: one volume of 2.5% glutaraldehyde, four volumes of 0.4 M cacodylate buffer, and five volumes of seawater (1.120 mOsm) (Ereskovsky et al., 2007), and then were post-fixed in 1% OsO4 in 0.2M Na-cacodylate buffer (pH 7.3) for 1 h. Further processing has been conducted as described in Fritzenwanker et al. (2007). Samples for SEM were

examined by the CamScan S-2 and JSM-6380LA scanning electron microscopes.

2.1. Model

2.1.1. Geometry

To describe the dynamics present during the gastrulation of *Clytia* we adapted the cell-boundary model of Tamulonis et al. (2011). The model is initialized with 134 wedge shaped cells, represented by an 85 vertex polygon and positioned in a circle, forming the blastula. The blastula is initialized as 260 μm in diameter, and the blastoderm is 20 μm thick, Fig. 3-A.

To estimate embryo dimensions for these simulations we measured the length and width of 17 live blastula stage embryos before and after compaction from light microscope (Olympus BX51) DIC images using Image J software. The length was taken as the longest dimension of the embryo and the width as the longest perpendicular transect to this. Embryo diameter was estimated as the average of the height and width. The number of cells around the embryo circumference was estimated from confocal microscope sections running through the oral-aboral axis, selected from confocal z-stacks. From images of two early gastrula stage embryos stained with phalloidin (cell boundaries) and Hoechst (nuclei) we counted 134 and 157 blastoderm cells, discriminated by the presence of an apical nucleus. Blastoderm thickness was estimated from the same confocal images as 22–26 μm. The length of filopodia in migrating cells estimated from SEM images was generally less than 5 μm but quite variable, with some reaching 10 μm (see Fig. 4C; other examples in Kraus et al., 2019; e.g. Fig. 5J).

Cells are tightly bound to their neighbours with vertices 1 and 75, mimicking apical junctions. Cells also have a strong apical belt, connecting vertices 1 and 75, which controls the apical size of cells. The cells are then divided into two populations: cells 1–35 become presumptive endodermal cells, while the rest, cells 36–134, become presumptive ectodermal cells. Nearly all properties of presumptive endodermal and ectodermal cells are the same, apart from that endodermal cells have no adhesive capabilities and are capable of forming filopodia once ingressed.

Unless otherwise specified, the default values of the model parameters are specified in Table 1.

Three distinct processes are modeled of the development of a *Clytia hemispherica* embryo; compaction, ingression, and intercalation. During the first process, compaction, all cells gradually increase the strain on their apical belt. This results in the blastula diameter decreasing, and the blastoderm thickness increasing. This change in shape results in enough strain on the cell membranes for bottle cells to form. Stochastically, endodermal bottle cells increase their apical strain even further, and detach from their neighbours. These old neighbours then directly form a junction, bridging the gap the ingressing cell left. Once a presumtpive endodermal cell ingressed, it is capable of forming filopodia. To model mediolateral mesenchymal intercalation, directed by PCP, filopodia are constrained in their slope, see section 2.1.6.

2.1.2. Dynamics

The forces are governed by simple Newtonian kinematics, where the force is equal to the mass × acceleration:

$$\mathbf{F} = ma \tag{1}$$

where each vertex has mass 1, making the force equal to the second derivative; acceleration. The force, *F*, can be split into several subparts:

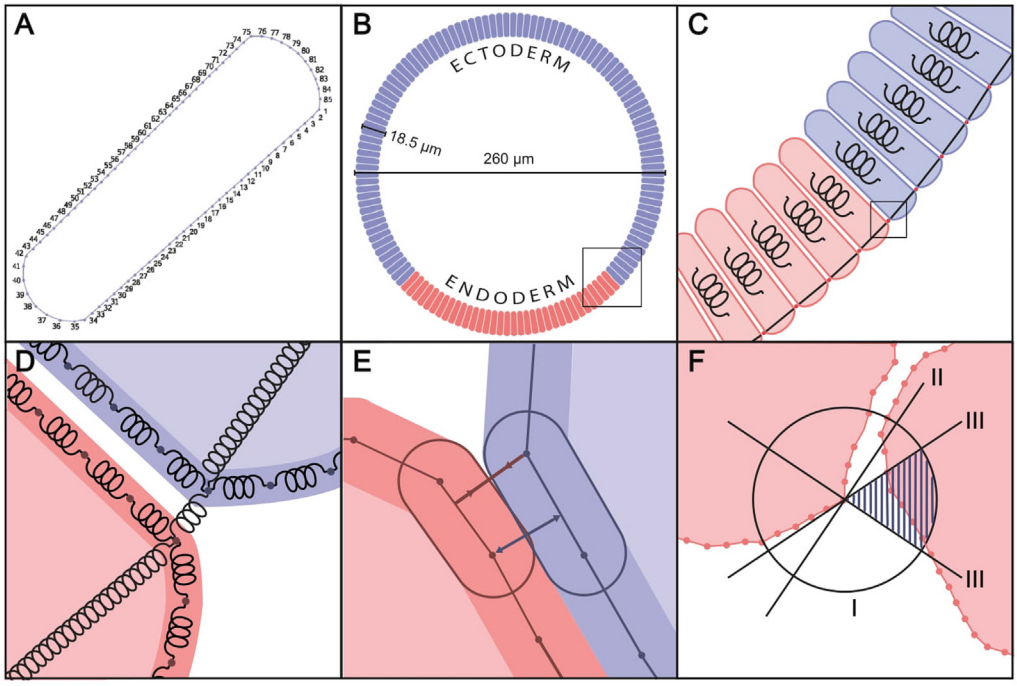

Fig. 3. Model architecture of *Clytia hemisphaerica* gastrulation. (A) Each cell is modeled as a polygon of 85 vertices. (B) The blastula is composed of a hollow ring of 134 identically shaped cells split into two distinct domains: the ectoderm (blue) and endoderm (red). The endoderm consists of 35 cells, and the ectoderm of 108, totalling 134 cells. (C) Each cell has an elastic cytoplasm. All the cells are connected apically (red dots), and have a spring across their apical diameter, black line. (D) Each cell is modeled as a set of springs connected in series, and is connected to its neighbours by a single spring at vertices 1 and 75. Vertices 1 and 75 of a single cell are also directly connected by a spring for apical strain. (E) Contact between cells is modeled as an elastic force between edges and vertices. In the image the red and blue cells are adhesive, and the red edge is attracting a blue vertex to its surface through adhesion (red arrows); whereas the blue edge is repulsing a slightly overlapping red vertex (blue arrows). (F) Decision boundary for the formation of a filopodium, illustrated for a vertex on the left cell. The circle (I) represents the maximum filopodia range, the diagonal line (II) assures that the filopium forms outside the cell, and the two mirrored lines (III) define the zone for lateral interactions imposed by PCP. Dark blue hatching indicates the region where all criteria apply to allow filapodium-mediated attraction between cells.

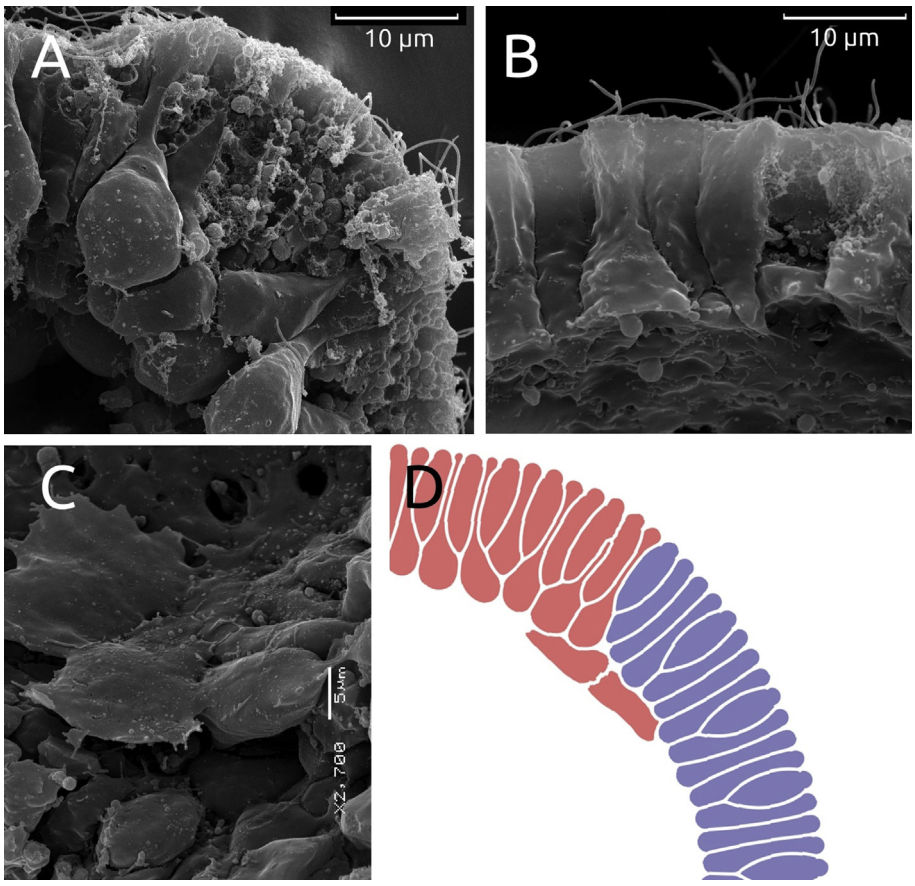

Fig. 4. Cell ingression observed by SEM (A–C) and simulation (D). A: High magnification of the oral area of the mid-gastrula stage embryo, several bottle cells are visible. B: Cells at the blastocoel roof remain ordered. C: Migrating ingressed cells. D: Simulated cell shapes (filopodia not visualized).

$$\mathbf{F} = \mathbf{F}_{spr} + \mathbf{F}_{cyt} + \mathbf{F}_{con} + \mathbf{F}_{fil} + \mathbf{F}_{vis} \tag{2}$$

specifying the vector forces of respectively the springs, cytoplasm, contact, filopodia, and the system's viscosity. Running a simulation step consists of determining the forces acting on each vertex and solving the resulting system of differential equations using the Velocity Verlet numerical integration method (Frenkel and Smith, 2002).

2.1.3. Springs

The cell membrane, cell junctions, and apical belt are governed by linear springs. The force of the springs is calculated by taking the strength of the stretch, and multiplying it with the direction of the stretch:

$$\mathbf{F}_{spr} = f \cdot \widehat{f} \tag{3}$$

Springs are restorative, meaning they try to maintain their rest length. The strength of the spring can be calculated as such:

$$f = k \frac{|\mathbf{r}_i - \mathbf{r}_j| - l_0}{l_0} \tag{4}$$

where k is the spring's stiffness, $|\mathbf{r}_i - \mathbf{r}_j|$ the distance between vertex i and j, and l_0 the spring's rest length. The rest length is parameterized by s

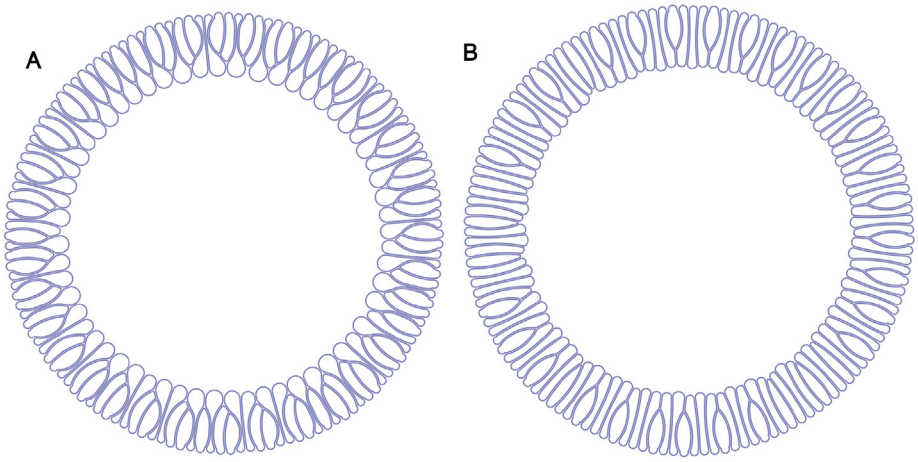

Fig. 5. Stills from simulations after compaction. A: adhesion $\alpha = 0$, B: $\alpha = 5$.

Table 1
Default model parameters.

Parameter			Value
Integration	Timestep, Δt		0.1
	Viscosity, η		1
Embryo	Diameter		260 μm
	Thickness		20 μm
	No. of cells	Ectoderm	89
		Endoderm	35
Springs	Stiffness, k	Membrane	1
		Junctions	25
		Belt	100
	Strain Factor, s	Membrane	0.3
		Junctions	0
		Belt	0.375
Cytoplasm	Stiffness, k_A		60
Repulsion	Range, h		0.75 μm
	Strength, R		5
Adhesion	Range, a		0.5 μm
	Strength, α	Ecto-Ecto	5
		Ecto-Endo	0
		Endo-Endo	0
Filopodia	Period, T_1		10
	Range, ρ		10 μm
	Force, ω		0.3
	Duration, T_2		50
	Direction, γ		0.66

such that $l_0 = (1-s)L_0$ where s is called the "strain factor" and $0 \leq s < 1$, and L_0 is the initial length of the edge.

The direction of the force can simply be calculated by taking the unit vector of the difference of the vertices:

$$\widehat{f} = \frac{\mathbf{r}_i - \mathbf{r}_{i-1}}{|\mathbf{r}_i - \mathbf{r}_{i-1}|} \tag{5}$$

The strain of the membrane is set so that if a cell forms a perfect circle, the membrane is at rest. The cell junctions and apical belt are initially at rest, with a strain of zero, with the apical belt increasing its strain over the time of the simulation.

2.1.4. Cytoplasm

The cytoplasm of the polygon is modeled as a linearly elastic fluid, so that the pressure the cytoplasm exerts is defined as the difference between the current volume (V) and the rest volume (V_0) times the cytoplasm stiffness. The volume of the cell can be calculated by applying Green's theorem to our polygon's coordinates:

$$V = -\frac{1}{2}\sum_{i=1}^{n} \mathbf{r}_{i,x}\cdot\mathbf{r}_{i+1,y} - \mathbf{r}_{i+1,x}\cdot\mathbf{r}_{i,y} \tag{6}$$

The total cytoplasm pressure is calculated as:

$$E_V = \frac{1}{2}k_V\left(\frac{V-V_0}{V}\right)^2 \tag{7}$$

with k_V as cytoplasm stiffness, and V_0 the rest volume of the cell. For all simulations V_0 is set to the volume the cell has at initialization.

The volume pressure can be translated into vertex forces by taking the gradient of the volume energy, for vertex i:

$$\mathbf{F}_{cyt} = -\nabla_i E_V = -k_V\frac{V-V_0}{V_0}\langle \mathbf{r}_{i-1,y} - \mathbf{r}_{i+1,y}, \mathbf{r}_{i+1,x} - \mathbf{r}_{i-1,x}\rangle \tag{8}$$

2.1.5. Contact

Interaction between edges are defined as edge-vertex pairs. A vertex that enters an edge's exclusive area is repelled from the capsule. Once a vertex entered this exclusive area, and the cells are adhesive, they adhere to each other, simulating the effect of cell adhesion molecules. The repulsion/adhesion force intensity is given by:

$$f = \begin{cases} -R\dfrac{d-h}{h} & 0 < d \leq h \\ -\alpha\left(1 - \dfrac{2}{a}\left|d - \left(h + \dfrac{a}{2}\right|\right)\right) & h < d \leq a+h \end{cases} \tag{9}$$

where d is the length of the displacement vector between the edge and the vertex, h the capsule diameter, a the adhesive area's diameter, α the adhesion strength, and R the repulsion strength.

The direction of the force is along the direction of the displacement vector, which is the shortest vector connecting the edge to the vertex. The displacement vector $\mathbf{d}$ between and edge $\mathbf{e} = \mathbf{r}_j - \mathbf{r}_i$ and vertex $\mathbf{r}_k$ is given by:

$$\mathbf{d} = \begin{cases} \mathbf{r}_k - \mathbf{r}_i & u \leq 0 \\ \widehat{\mathbf{e}} \times \mathbf{r}_k - \mathbf{r}_i \times \widehat{\mathbf{e}} & 0 < u < 1 \\ \mathbf{r}_k - \mathbf{r}_j & u \geq 1 \end{cases} \tag{10}$$

where $\widehat{\mathbf{e}} = \mathbf{e}/||\mathbf{e}||$ is the normalized edge vector and

$$u = \frac{(\mathbf{r}_k - \mathbf{r}_i)\cdot\mathbf{e}}{\mathbf{e}\cdot\mathbf{e}} \tag{11}$$

is the normalized projection of the vertex onto the edge. If $u \leq 0$ or $u \geq 1$, then the intruding vertex $\mathbf{r}_k$ is touching one of the capsule's rounded ends and is only interacting with one of the two edge's vertices. Otherwise it is touching the edge, and interacting with both vertices simultaneously:

	F_{cont_k}	F_{cont_i}	F_{cont_j}
$u \leq 0$	$f_i\widehat{\mathrm{d}}$	$-f_i\widehat{\mathrm{d}}$	0
$0 < u < 1$	$f_i\widehat{\mathrm{d}}$	$-(1-u)f_i\widehat{\mathrm{d}}$	$-uf_i\widehat{\mathrm{d}}$
$u \geq 0$	$f_i\widehat{\mathrm{d}}$	0	$-f_i\widehat{\mathrm{d}}$

(12)

2.1.6. Filopodia

Cells can form filopodia as a means of long-range cell-cell interactions. We model filopodia extension and adhesion as a stochastic process in which cells pulls on other cells within a given range. Once a filopodium formed between, e.g. vertex $\mathbf{r}_i$ and $\mathbf{r}_k$, it exerts a constant pulling force on both vertices for duration T_2:

$$\mathbf{F}_{fil} = \omega\frac{\mathbf{r}_k - \mathbf{r}_i}{|\mathbf{r}_k - \mathbf{r}_i|} \tag{13}$$

where ω is the strength of the filopodia.

Filopodia can form between two vertices if;

- the cell initializing the filopodium is endoderm, and has ingressed,
- the vertices belong to different cells,
- the vertices are within range of each other,
- the vertices are not adhering to other vertices,
- the vertices are not bound to another filopodium,
- the filopodium forms outwards of both cells

Whether a filopodium will be outwards can be determined with the indicator function described in equation (14):

$$f(i,k) = \begin{cases} \text{True} & \text{if } (\mathbf{r}_{i+i} - \mathbf{r}_{i-i}) \times (\mathbf{r}_k - \mathbf{r}_i) > 0 \\ \text{False} & \text{otherwise} \end{cases} \tag{14}$$

To model the forming of mediolateral bonds, guided by PCP, a constraint on the slope of the filopodia can be added. If the slope m is $-\gamma \leq m \leq \gamma$, the filopodium follows the direction of PCP and is valid when PCP is modeled. Furthermore the formation of filopodia is stochastic, and is governed by the Poisson distribution. On average, one filopodium forms every λ per endodermal cell, and a random, admissible, combination of vertices is chosen.

2.1.7. Viscosity

Viscosity, the system's damping, is modeled as a force acting opposite

to the motion of each vertex:

$$\mathbf{F}_{vis_i} = -\eta_i \mathbf{v}_i = -\eta_i \frac{\Delta \mathbf{r}_i}{\Delta t} \quad (15)$$

where η is the system's viscosity.

2.2. Implementation

The model was implemented with Python3.7, relying on numpy and numba for respectively CPU and GPU optimization. Visualization was done with matplotlib.

3. Results

3.1. Overview of cell shape changes during compaction and ingression

Prior to gastrulation, the epithelializing blastula undergoes process that we term "compaction" (see Introduction and Fig. 1). Compaction reduces the diameter of the blastula markedly between around 7 and 9 hpf, from about 260 μm to 230 μm in diameter (n=17 embryos, standard deviations 37 μm and 25 μm respectively). As the overall diameter of the embryo decreases, the epithelial cells become more elongated whilst presumably maintaining their approximate volume. This morphogenetic change is likely to be linked to the development of apical contractility of individual cells following their epithelialization and apicobasal polarization. Consistent with this, the intensity of actin filament staining in the apical cortex increases markedly between the mid and late blastula stages (compare panels C and K in Fig. 3 in Kraus et al., 2019). The elongation of the cells results in an increased circumference in the apicobasal plane, which is predicted to cause strain on the cortex.

The cell and embryo shape changes observed in *Clytia* during gastrulation are summarized here from the detailed description by Kraus et al., 2019. Through the compaction process regularly interspersed cell populations across the embryo segregate progressively, showing two basic morphologies, as previously described in presumptive endodermal domain of *Nematostella* blastulae (Tamulonis et al., 2011). Some cells develop a swelling of the basal region, whilst neighboring cells become "bottle cells" tapering from apical to basal (Figs. 4 and 5). At the start of gastrulation, a subpopulation of cells in the oral domain starts to undergo epithelial-mesenchymal transition (EMT), ahead of ingression into the blastocoel. In a classical process of EMT, these presumptive endodermal cells pass through a characteristic "bottle cell" stage, involving extreme narrowing of the apical part of the cell to form a narrow neck region and migration of the nucleus from the apical pole to the expanding basal "bulb". These bottle cells likely derive from the population of "basally swollen" cells at the blastula stage, however this requires experimental confirmation eg by live imaging approaches. EMT of the bottle cells in the oral domain is completed by detachment into the blastocoel and migration towards the aboral pole.

Around 11 hpf at 18 $^{\circ}C$ an accumulation of cells is visible, corresponding to the ingressing endodermal cells at the oral pole. The extent of ingression increases throughout gastrulation, whilst the width of the gastrula decreases. The embryo becomes less spherical, elongating progressively along the future oral-aboral axis.

From the late blastula stage, mitotic cells are observed only rarely in any cell layer. Cell proliferation is thus highly unlikely to affect morphogenesis during gastrulation.

3.2. Simulation

To simulate these morphogenetic changes of the *Clytia* embryo from early blastula to the end of gastrulation, we adapted the cell boundary-based model devised by Tamulonis et al. for *Nematostella* embryogenesis. We set the dimensions of the blastula starting condition to those measured using biological material (see Materials and Methods). Conditions of low adhesion combined with lateral constraint and apical contraction promoted the appearance of cells with basal expansions in the blastoderm, interspersed with squat cells Fig. 5. These conditions closely resemble those that promote bottle cell formation in the *Nematostella* simulation (Tamulonis et al., 2011).

To simulate gastrulation of the late-stage blastula we continued with the settings of compaction , but modified two parameters for cells in the oral domain (i.e. presumptive endoderm cells): We set cell-cell adhesion to zero, and let apical constriction of basally-expanded cells further increase. This promoted the "basally expanded" cells in this domain to transform further into bona fide bottle cells. Critically, the model allows them to detach from the epithelium once their apical surface passed a threshold value (1 μm). These simple changes generate cellular behaviour in the model very similar to those observed in vivo in *Clytia hemisphaerica* embryos, Fig. 4.

In the model described so far we established parameters in which all cells of the blastoderm undergo apical surface contraction, ectodermal cells adhere to each other, endodermal cells have no adhesive properties, and endodermal bottle cells continue apically constricting and allow some of them to detach from the epithelium. To test whether this could account for inward migration of the ingressed cells, we added to the model the ability of ingressed cells to form filopodia orthogonal to the oral-aboral axis. When simulations were run including this factor promoting lateral interactions, these cells started migrating along the blastocoel wall to completely fill the blastocoel, Fig. 6 and supplementary data.

3.3. Parameter space

The model shows the same qualitative properties in terms of morphology changes for a wide range of different parameter settings. These morphologies could, however, be changed modifying four key parameters: the size of the oral domain, the adhesivity of the presumptive endoderm cells, the PCP parameter defining the orientation of filapodia and "boundary capture" between ectodermal and endodermal cells, Fig. 7.

Concerning oral domain size, we observed that increasing the number of endodermal cells that can ingress (top row in Fig. 7) caused the final embryo morphology to become rounder. This can be understood intuitively as a circle has a greater area than an oval with the same circumference. As more endodermal cells ingress, this effect is reinforced because the number of cells in the outer epithelium decreases. This resembles the living phenotype observed when the size of the oral domain is increased experimentally by knockdown of the aboral fate regulator Fz3 (Momose and Houliston, 2007).

Concerning the adhesion between presumptive endoderm cells, increasing the adhesivity factor in the model reduced the ability of ingressed cells to migrate, and rendered the mediolateral intercalation process less effective (Fig. 7 middle row). When adhesive properties were increased maximally in this domain, bottle cell formation did not occur and the ingression process was completely blocked. On the other hand, reducing the strength of the filopodia (ω), did not prevent gastrulation, although the pear-shape seen in many mid-gastrula embryos (Fig. 1 16.5hpf, Fig. 6E, Kraus et al., 2019 Figs. 6b and 7c) did not occur in the simulations (not shown).

Concerning PCP, when the polarized directionality of endodermal cell filopodia was substantially disrupted, elongation of the embryo in the simulation was reduced and the blastocoel failed to fill completely, resulting in a circular hollow bilayer (Fig. 7K–O). This is strikingly similar to the phenotype observed when the PCP protein Strabismus is disrupted experimentally (Momose et al., 2012). Finally, boundary capture between endodermal and ectodermal cells was found to be required for successful gastrulation in our model. When endodermal cells were allowed only to form filopodia with other endodermal cells, they organized into a central column but the embryo did not elongate and the blastocoel did not completely fill.

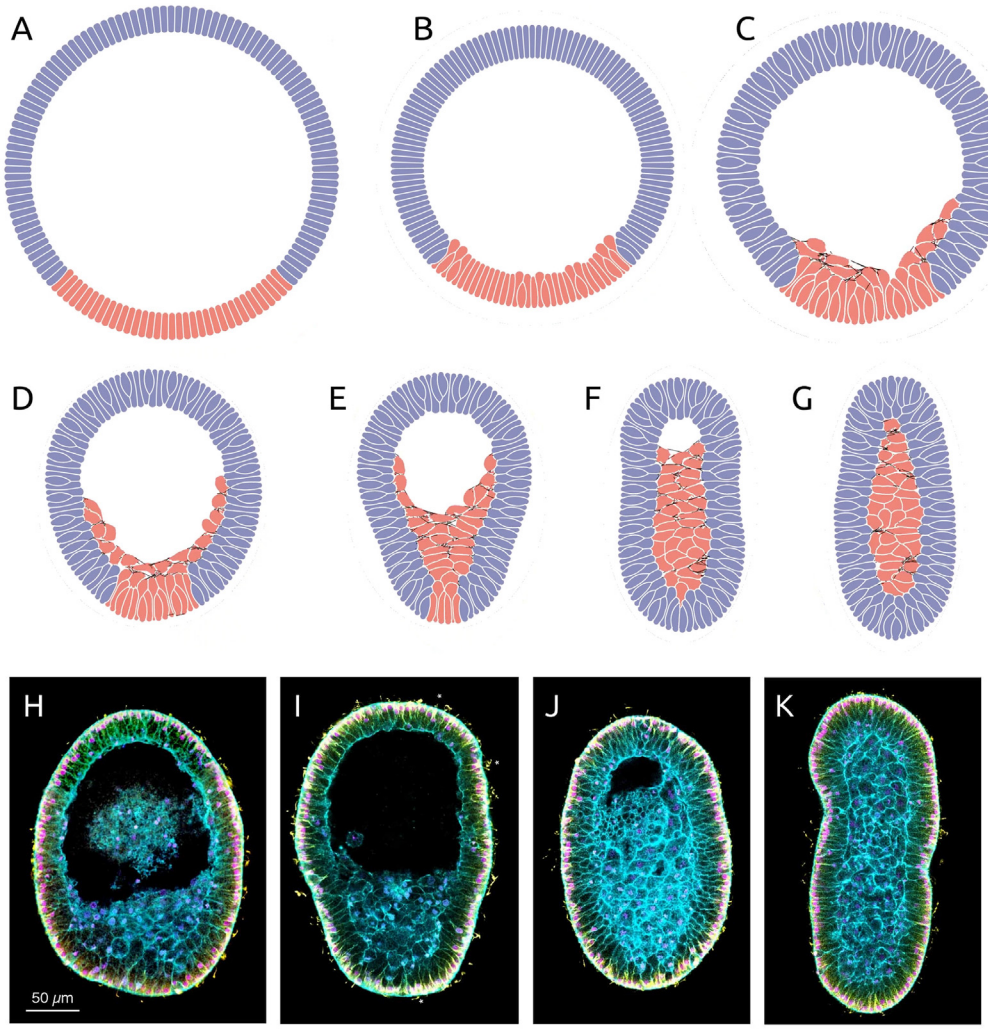

Fig. 6. Comparison between simulation with default parameters, and real embryos. (A–G) Blue cells represent ectodermal cells, and red cells presumptive endodermal cells. (A) The model initial state, with each subsequent image corresponding to roughly an increase of one real-time hour, or 20 model "minutes". (B) After compaction, reduced cell adhesion causes bottle cell formation first in the oral domain/presumptive endoderm cells (red). (C–F) Bottle cells in the oral domain start ingression and through lateral filapodia (black lines) they migrate along the blastocoel wall. In frame (E) the gastrula wall bends around the center. (G) The blastocoel is completely filled and the oval shape elongated. (H–K) Confocal images of embryos fixed respectively at early, early/mid, mid, and late stages of gastrulation. Scale bar 50 μm. The oral pole is at the bottom in all embryos.

3.4. Critical parameter differences between Nematostella and Clytia simulations

Our original *Nematostella vectensis* gastrulation simulation recapitulates gastulation based on cell sheet invagination whereas the one developed here for *Clytia hemisphaerica* recapitulates gastrulation by unipolar cell ingression, resulting in a very different embryo morphology. To explore which aspects of the simulations are most critical for determining these two gastrulation modes we tested the effects of varying different parameters, starting with the initial conditions determined for *Nematostella* (87 cells, gastrula diameter 200 μm and 32 μm thick) rather than *Clytia* embryos (Fig. 8; tested parameters summarized in Table 2).

We found that to generate *Clytia*-like gastrulation by unipolar cell ingression from the established *Nematostella* model for gastulation by oral blastoderm invagination (endpoint shown in Fig. 8A) required three principal changes: reducing the number of presumptive endodermal cells, expanding the domain of cortical contraction, and allowing cell ingression. Applying apical contraction to all cells (using the lower *Clytia* value) rather than restricting this to the oral domain generated a spherical compact blastula comprising basally expanded and squat cells across all regions, abolishing involution (Fig. 8D). Allowing cell ingression then drove completion of gastrulation (Fig. 8E), with lateral 'PCP' interactions between endoderm cells required for morphogenesis, where a reduction in the number of presumptive endodermal cells is required for a torpedo shaped gastrula (Fig. 8F, see also Fig. 7A–E, K–N). In contrast, reducing the strength of apical constriction to the lower, *Clytia* model, value while maintaining the *Nematostella*-model restriction to the oral domain was insufficient to drive gastrulation by either invagination or ingression (Fig. 8B). This simulation illustrates the importance of global embryo "compaction" for sustaining cell ingression by maintaining tension within the system. It generated a flattened blastula-like morphology including bottle cells located within a 'floor plate', but gastrulation stalled when these bottle cells were allowed to ingress (Fig. 8G) because their loss from the blastoderm causes the system to relax and return to a configuration comprising less extreme forms of bottle and squat cells, unable to support further ingression. Allowing bottle cell ingression in the *Nematostella* model resulted in a composite embryo morphology showing both invagination and ingression, as seen during gastrulation in the anthozoan *Haliplanella lineata* (Fukui, 1991) (Fig. 8C).

4. Discussion

Simulations run using the cell-based boundary model that we present here capture many qualitative features of *Clytia* gastrulation. We found the model definitions were very similar to those used for *Nematostella*, despite the very different gastrulation modes used in these species. The main differences in the models were as follows: In the *Clytia* model, apical constriction occurs in all cells in the blastoderm prior to gastrulation, introducing strain to the cortex of each cell, whereas in *Nematostella* apical constriction is restricted to the oral domain. In both models, down-regulation of cell-cell adhesion for endodermal cells

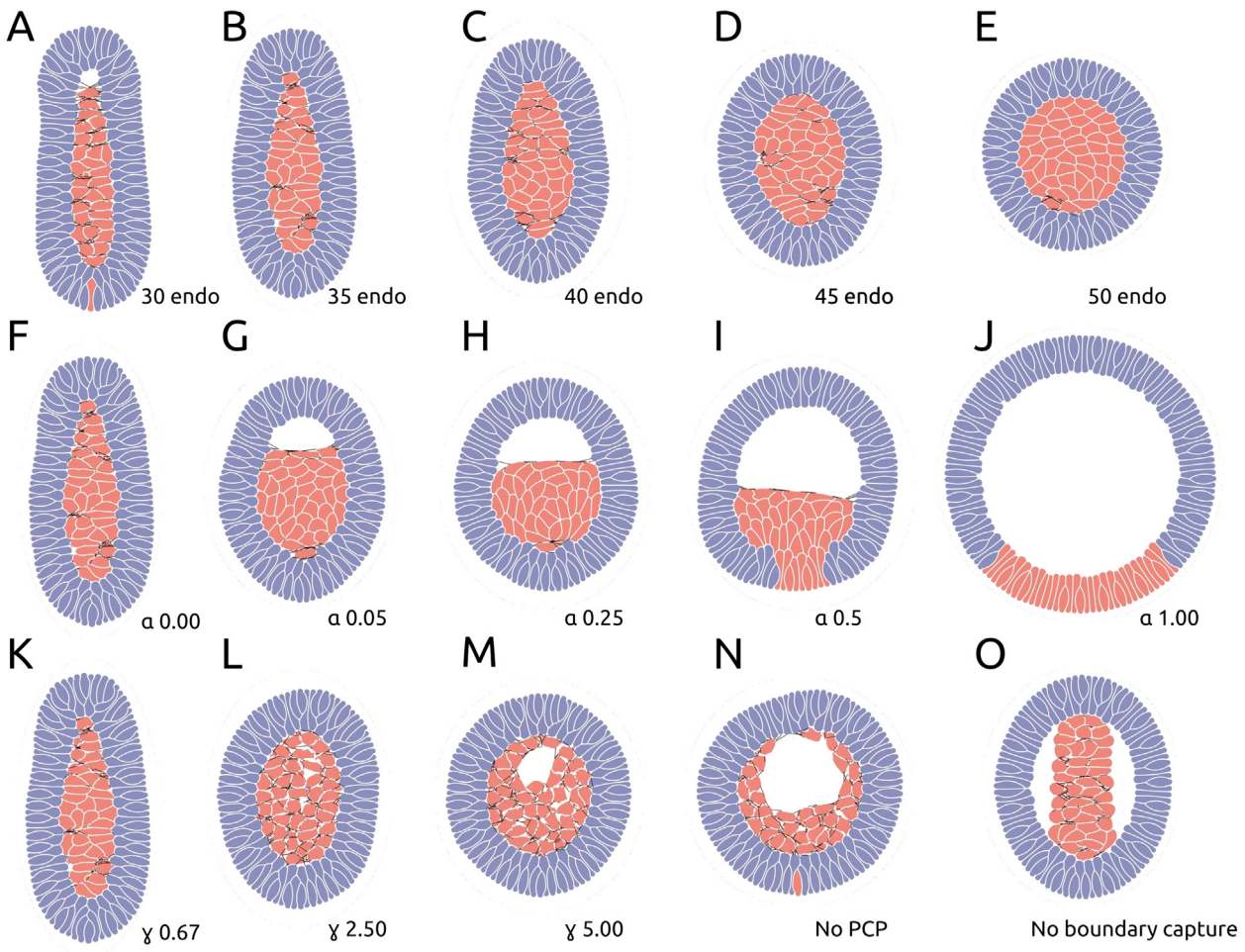

Fig. 7. Parameter sweeps. End points of simulations run using different parameters. In each row a single parameter was varied, while the other parameters were set to their default values. In the first row the size of the oral domain, ie the number of presumptive endodermal cells, is varied. In the second row endodermal cell-cell adhesion was increased. In the third row PCP was gradually decreased. In frame O endodermal cells only form filopodia with other endodermal cells, not with ectodermal cells. Note that B, F, and K are the same image.

promotes bottle cell formation, however in the *Clytia* but not in the *Nematostella* model, these bottle cells can break apical junctions with their neighbours, allowing them to migrate inwards. In both *Clytia* and *Nematostella* models a long-range gap-bridger property induced by endodermal cells was introduced as filopodia. The critical differences in cell properties underlying the two gastrulation modes was confirmed by running simulations using the *Nematostella* embryo starting configuration (Fig. 8). Extending the spatial domain of apical cell constriction across the embryo, and subsequently weakening cell adhesion within the presumptive endoderm domain could switch the gastrulation mode from cell sheet invagination to unipolar cell ingression. Allowing in addition PCP directed interactions between the ingressing cells promoted the characteristic elongated morphology of the *Clytia* planula.

Our model leads us to propose that the key cellular processes necessary and sufficient for driving gastrulation in *Clytia* are apical constriction of all cells of the blastula, then reduced cell-cell adhesion and cellular ingression (ie loss of apical contacts below a threshold apical width) in the oral domain, and finally mediolateral intercalation of ingressed cells the presumptive endoderm. Compaction driven by apical constriction emerges as a likely prerequisite for bottle cell formation by generating the required strain on the epithelium. It would be interesting to explore experimentally this hypothesis by blocking compaction, or lowering cell-cell adhesion across the blastula. Disruption of PCP during *Clytia* gastrulation is known to have profound effects on the morphology of the late gastrula, with morpholino-mediated downregulation of Strabismus or Dishevelled expression reducing embryo elongation and the extent of cell ingression during gastrulation (Momose et al., 2012). Embryo morphologies predicted by model simulations while tuning the PCP parameter (Fig. 1 bottom row), were highly reminiscent of these PCP down-regulation phenotypes. Specifically, our model predicts that the embryo will adopt a less elongated shape as endodermal cell PCP decreases, supporting the hypothesis that PCP-mediated mediolateral intercalation contributes significantly to embryo elongation during gastrulation. Using our 2D model we cannot address the hypothesis that mediolateral intercalation between cells of the ectoderm as well as in the endoderm contributes to embryo elongation. Intercalation of ectodermal cells, either a passive or active nature, obligatorily accompanies the change in embryo shape from spherical to elongated, and has been demonstrated by cell tracing in another *Clytia* species (Byrum, 2001). Intercalation in 3D likely accounts for the difference in final length between the real embryo and our 2D simulation. To determine whether epithelial intercalation plays an active role during *Clytia* gastrulation, the key cellular behaviors and underlying parameters that we have defined will need to be incorporated into a 3D model.

In conclusion, cell-based boundary models show great promise in the modeling of mechanical cellular processes, and can faithfully simulate many of the features of hydrozoan gastrulation by unipolar cell ingression. In the current model, gene regulation defining the oral domain downstream of Wnt signalling has been modeled implicitly by giving the oral domain and ectodermal cells different parameters from the start of

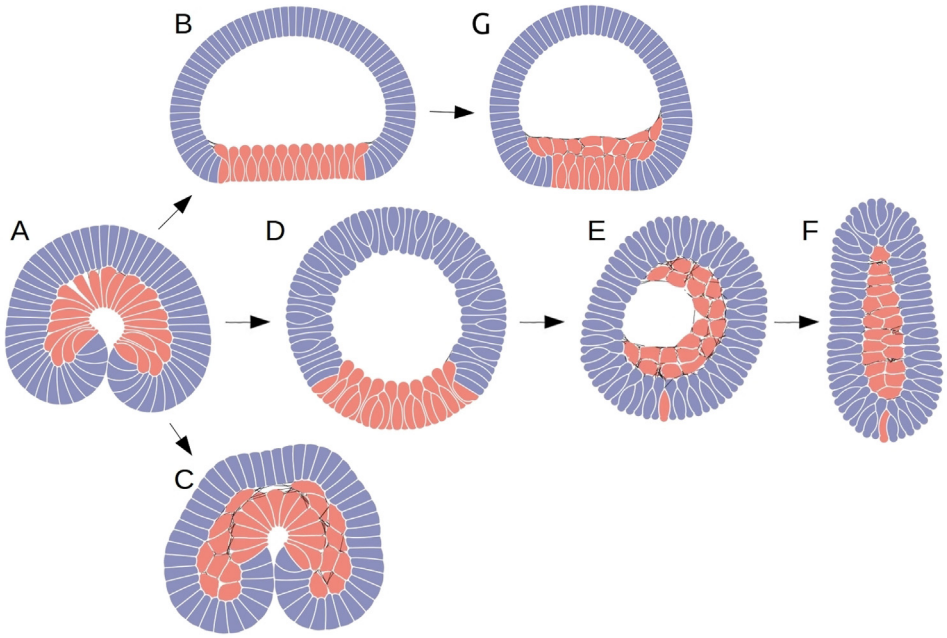

Fig. 8. Exploration of the model parameters that could explain the difference in morphology between *Nematostella vectensis* and *Clytia hemisphaerica* post-gastrulation embryos. Simulation end-points are shown in all cases, starting with cell numbers and dimensions determined from *Nematostella*. Arrows indicate the transformations provoked by changing a single parameter as detailed below. (A) The default settings established for *Nematostella* by Tamulonis et al. (B) Reducing only the value for apical cell constriction strength resulted in reduced invagination. (C) Allowing cell ingression in the presumptive endoderm domain resulted in a composite embryo morphology. (D) Applying the same weak apical constriction as in B to all cells rather than restricting this to the oral domain produced a configuration very similar to that observed in our *Clytia* simulation, despite the cell number and dimension difference. (E) In a context of global apical constriction, allowing bottle cells to reduce apical connections promotes unipolar cell ingression. (F) Constraining interactions between ingressing cells laterally (PCP) mediates the narrowing of the embryo to a torpedo shape. (G) Allowing bottle cells to ingress alone is not enough for complete ingression of the presumptive endodermal cells. The parameters used for each simulation are summarized in Table 2.

Table 2
Model parameters of Fig. 8.

Parameter			A	B	C	D	E	F	G
Embryo	Diameter		200	200	200	200	200	200	200
	Thickness		32	32	32	28	28	28	32
	No. of cells	Ectoderm	63	63	57	63	67	67	63
		Endoderm	24	24	30	24	20	20	24
	Ingression		N	N	Y	N	Y	Y	Y
Springs	Strain, s	Belt	0.65	0.375	0.65	0.375	0.375	0.375	0.375
Filopodia	Direction, γ		N	N	N	N	N	0.66	N

the simulation. In the future an integrated model for *Clytia* gastrulation could be built upon this framework by integrating data on gene expression and gene regulatory networks, and could serve to test the spatial and temporal consequences of gene interactions as envisaged by Abdol et al. (2018) for *Nematostella*. More widely, since models of this type do not compromise on resolution, they can be used to explore virtually any morphogenetic process involving changes in cellular boundary properties and cell shape. Using these models to explore other modes of gastrulation, including delamination, epiboly and involution, could provide insight into whether these processes differ fundamentally, and in what respects they are based on a suite of similar cellular properties. From our simulations we predict that there will be critical differences in the effector genes regulated by transcription factors activated dowstream of Wnt/Beta -catenin signalling in the oral domain of the embryo in different cnidarian species. In *Nematostella* but not in *Clytia*, we would expect activation of apical cortex constriction to be restricted to this domain, and cell adhesion genes conversely to be more strongly down-regulated downstream of Wnt signalling in *Clytia* than in *Nematostella*.

Acknowledgements

We thank our research colleagues at the LBDV, especially Tsuyoshi Momose for their previous work on *Clytia* to provide the experimental foundations of this study, as well as for many useful discussions. We also thank Alexandre Jan and Laurent Gilletta for animal maintenance. Experimental work was supported by core CNRS and Sorbonne University funding to the LBDV. The Marine Resources Centre (CRBM) and PIV imaging platform of Institut de la Mer de Villefranche (IMEV) used in this study are supported by EMBRC-France (#ANR-10-INBS-02). SEM was performed at the Electron Microscopy Laboratory of the Shared Facilities Center of the Moscow State University. We would like to thank two of the anonymous reviewers for their constructive comments, one of the comments resulted in an extended parameter sweep which provided us with some new valuable insights.

Appendix A. Supplementary data

Supplementary data to this article can be found online at https://doi.org/10.1016/j.ydbio.2019.12.012.

References

Abdol, A., Bedard, A., Lánský, I., Kaandorp, J., 2018. High-throughput method for extracting and visualizing the spatial gene expressions from in situ hybridization images: a case study of the early development of the sea anemone Nematostella vectensis. Gene Expr. Patterns 27, 36–45. https://doi.org/10.1016/j.gep.2017.10.005. http://www.sciencedirect.com/science/article/pii/S1567133X17301151.

Byrum, C., 2001. An analysis of hydrozoan gastrulation by unipolar ingression. Dev. Biol. 240 (2), 627–640. https://doi.org/10.1006/dbio.2001.0484. http://www.sciencedirect.com/science/article/pii/S0012160601904841.

Ereskovsky, A.V., Tokina, D.B., Bézac, C., Boury-Esnault, N., 2007. Metamorphosis of cinctoblastula larvae (homoscleromorpha, porifera). J. Morphol. 268 (6), 518–528. https://doi.org/10.1002/jmor.10506 arXiv. https://onlinelibrary.wiley.com/doi/pdf/10.1002/jmor.10506. https://onlinelibrary.wiley.com/doi/abs/10.1002/jmor.10506.

Frenkel, D., Smit, B., 2002. Chapter 4 - molecular dynamics simulations. In: Frenkel, D., Smit, B. (Eds.), Understanding Molecular Simulation, second ed. Academic Press, San Diego, pp. 63–107. https://doi.org/10.1016/B978-012267351-1/50006-7. second ed. Edition. http://www.sciencedirect.com/science/article/pii/B9780122673511500067.

Fritzenwanker, J.H., Genikhovich, G., Kraus, Y., Technau, U., 2007. Early development and axis specification in the sea anemone Nematostella vectensis. Dev. Biol. 310 (2), 264–279. https://doi.org/10.1016/j.ydbio.2007.07.029. http://www.sciencedirect.com/science/article/pii/S0012160607012171.

Fukui, Y., 1991. Embryonic and larval development of the sea anemone haliplanella lineata from Japan. Hydrobiologia 216 (1), 137–142. https://doi.org/10.1007/BF00026454.

Gilbert, S.F., 2010. Developmental Biology, ninth ed. Sinauer Associates.

Graner, F.m. c., Glazier, J.A., 1992. Simulation of biological cell sorting using a two-dimensional extended potts model. Phys. Rev. Lett. 69, 2013–2016. https://doi.org/10.1103/PhysRevLett.69.2013. https://link.aps.org/doi/10.1103/PhysRevLett.69.2013.

Houliston, E., Momose, T., Manuel, M., 2010. Clytia hemisphaerica: a jellyfish cousin joins the laboratory. Trends Genet. 26 (4), 159–167. https://doi.org/10.1016/j.tig.2010.01.008. http://www.sciencedirect.com/science/article/pii/S0168952510000235.

Kraus, Y.A., Markov, A.V., 2017. Gastrulation in cnidaria: the key to an understanding of phylogeny or the chaos of secondary modifications? Biol. Bull. Rev. 7 (1), 7–25. https://doi.org/10.1134/S2079086417010029.

Kraus, Y., Technau, U., 2006. Gastrulation in the sea anemone Nematostella vectensis occurs by invagination and immigration: an ultrastructural study. Dev. Gene. Evol. 216 (3), 119–132. https://doi.org/10.1007/s00427-005-0038-3.

Kraus, Y., Chevalier, S., Houliston, E.. Cell shape changes during larval body plan development in clytia hemisphaerica. bioRxivarXiv. https://www.biorxiv.org/content/early/2019/12/03/864223.full.pdf. https://www.biorxiv.org/content/early/2019/12/03/864223.

Lapébie, P., Ruggiero, A., Barreau, C., Chevalier, S., Chang, P., Dru, P., Houliston, E., Momose, T., 2014. Differential responses to Wnt and PCP disruption predict expression and developmental function of conserved and novel genes in a cnidarian. PLoS Genet. 10 (9), 1–23. https://doi.org/10.1371/journal.pgen.1004590.

Leclère, L., Horin, C., Chevalier, S., Lapébie, P., Dru, P., Peron, S., Jager, J., Condamine, T., Pottin, K., Romano, S., Steger, J., Sinigaglia, C., Barreau, C., Quiroga-Artigas, G., Ruggiero, A., Fourrage, C., Kraus, J., Poulain, J., Aury, J.M., Wincker, P., Quéinnec, E., Technau, U., Manuel, M., Momose, T., Houliston, E., Copley, R., 2019. The genome of the jellyfish *Clytia hemisphaerica* and the evolution of the cnidarian life-cycle. Nature Ecology and Evolution. https://doi.org/10.1038/s41559-019-0833-2.

Magie, C.R., Daly, M., Martindale, M.Q., 2007. Gastrulation in the cnidarian Nematostella vectensis occurs via invagination not ingression. Dev. Biol. 305 (2), 483–497. https://doi.org/10.1016/j.ydbio.2007.02.044. http://www.sciencedirect.com/science/article/pii/S0012160607001807.

Marco Scianna, K.W., Preziosi, Luigi, 2013. A cellular potts model simulating cell migration on and in matrix environments. Math. Biosci. Eng. 10, 235. https://doi.org/10.3934/mbe.2013.10.235, 1551–0018_2013_1_235. http://aimsciences.org//article/id/f177885a-006a-4b14-ab37-8096a72c798d.

Momose, T., Houliston, E., 2007. Two oppositely localised frizzled rnas as axis determinants in a cnidarian embryo. PLoS Biol. 5 (4), 1–11. https://doi.org/10.1371/journal.pbio.0050070.

Momose, T., Schmid, V., 2006. Animal pole determinants define oral–aboral axis polarity and endodermal cell-fate in hydrozoan jellyfish podocoryne carnea. Dev. Biol. 292 (2), 371–380. https://doi.org/10.1016/j.ydbio.2006.01.012. http://www.sciencedirect.com/science/article/pii/S0012160606000431.

Momose, T., Derelle, R., Houliston, E., 2008. A maternally localised wnt ligand required for axial patterning in the cnidarian clytia hemisphaerica. Development 135 (12), 2105–2113. https://doi.org/10.1242/dev.021543 arXiv. http://dev.biologists.org/content/135/12/2105.full.pdf. http://dev.biologists.org/content/135/12/2105.

Momose, T., Kraus, Y., Houliston, E., 2012. A conserved function for strabismus in establishing planar cell polarity in the ciliated ectoderm during cnidarian larval development. Development 139 (23), 4374–4382. https://doi.org/10.1242/dev.084251 arXiv. http://dev.biologists.org/content/139/23/4374.full.pdf. http://dev.biologists.org/content/139/23/4374.

Odell, G., Oster, G., Alberch, P., Burnside, B., 1981. The mechanical basis of morphogenesis: I. epithelial folding and invagination. Dev. Biol. 85 (2), 446–462. https://doi.org/10.1016/0012-1606(81)90276-1. http://www.sciencedirect.com/science/article/pii/0012160681902761.

Lapébie, P., Borchiellini, C., Houliston, E., 2011. Dissecting the PCP pathway: one or more pathways?: Does a separate Wnt-Fz-Rho pathway drive morphogenesis? Bioessays 33 (10), 759–768.

Szabó, A., Merks, R.M., 2013. Cellular potts modeling of tumor growth, tumor invasion, and tumor evolution. Front. Oncol. 3, 87. https://doi.org/10.3389/fonc.2013.00087. https://www.frontiersin.org/article/10.3389/fonc.2013.00087.

Tamulonis, C., Postma, M., Marlow, H.Q., Magie, C.R., de Jong, J., Kaandorp, J., 2011. A cell-based model of Nematostella vectensis gastrulation including bottle cell formation, invagination and zippering. Dev. Biol. 351 (1), 217–228. https://doi.org/10.1016/j.ydbio.2010.10.017. http://www.sciencedirect.com/science/article/pii/S0012160610011371.

Walck-Shannon, E., Hardin, J., 2014. Cell intercalation from top to bottom. Nat. Rev. Mol. Cell Biol. 15 (1), 34–48. https://doi.org/10.1038/nrm3723, 24355988[pmid]. http://www.ncbi.nlm.nih.gov/pmc/articles/PMC4550482/.

Wallingford, J.B., Fraser, S.E., Harland, R.M., 2002. Convergent extension: the molecular control of polarized cell movement during embryonic development. Dev. Cell 2 (6), 695–706. https://doi.org/10.1016/S1534-5807(02)00197-1. http://www.sciencedirect.com/science/article/pii/S1534580702001971.